Effect of Size-Selective Retention on the Cotransport of Hydroxyapatite and Goethite Nanoparticles in Saturated Porous Media

ARTICLE *in* ENVIRONMENTAL SCIENCE & TECHNOLOGY · JULY 2015

Impact Factor: 5.33

3 AUTHORS, INCLUDING:

Dengjun Wang

University of Delaware, Newark, DE 19716, USA

20 PUBLICATIONS **205** CITATIONS

SEE PROFILE

Deb P. Jaisi

University of Delaware

52 PUBLICATIONS **1,215** CITATIONS

SEE PROFILE

Environmental Science & Technology

Article

pubs.acs.org/est

Effect of Size-Selective Retention on the Cotransport of Hydroxyapatite and Goethite Nanoparticles in Saturated Porous Media

Dengjun Wang, Yan Jin,* and Deb P. Jaisi*

Department of Plant and Soil Sciences, University of Delaware, Newark, Delaware 19716, United States

Supporting Information

ABSTRACT: Attributable to their nanoscale size and slow phosphorus (P) release kinetics, hydroxyapatite nanoparticles (HANPs) are increasingly advocated as a promising P nanofertilizer. Additionally, HANPs have been extensively used to remediate soils, groundwater, and nuclear wastewaters contaminated with metals and radionuclides. Increasing application of HANPs for agronomic and environmental advantages will expedite their dissemination in subsurface environments. Because the biogeochemical cycling of P is intimately coupled with iron, it is anticipated that HANPs and released P from HANPs interact with iron oxides, particularly naturally occurring goethite nanoparticles (GNPs) because of their nanoscale size and high reactivity toward P. Here, we investigated the cotransport and retention of HANPs and GNPs in water-saturated sand columns under environmentally relevant transport conditions (pH and natural organic matter type and concentration). Our results indicated that the "size-selective retention", i.e., preferential retention of larger particles near the column inlet and elution of smaller particles occurred during cotransport of HANPs and GNPs, and the cotransport of both NPs is highly sensitive to solution chemistry that determines NPs dissolution, homo- and heteroaggregation, and co- and competitive-retention. These findings have important insights into application of HANPs as a promising P nanofertilizer and an in situ amendment for contaminated site remediation.

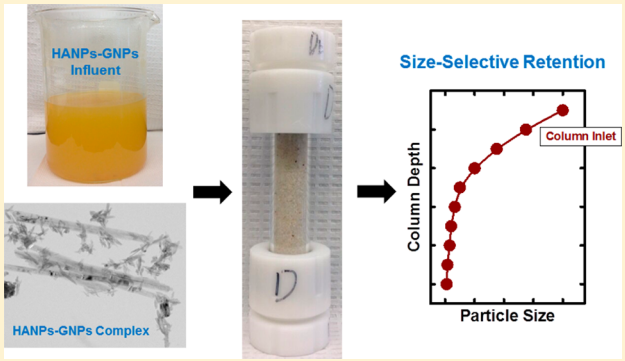

INTRODUCTION

Phosphorus (P) is a nonrenewable resource and an essential element for agricultural productivity.[1] To meet the increasing food demands of a rapidly growing population, application of P fertilizers has increased drastically after the green revolution.[1,2] However, a significant fraction of applied P to agricultural soils is inadvertently lost to open waters and has caused eutrophication.[3−5] This unintended consequence has promoted seeking new technology to limit P loss out of agricultural fields but without compromising crop yield. Owing to their nanoscale size, low leaching rate, and slow P release kinetics, hydroxyapatite nanoparticles (HANPs, $Ca_{10}(PO_4)_6(OH)_2$) are advocated as a promising P nanofertilizer[6−8] of lower loss risk and elevated output efficiency than conventional water-soluble P fertilizers.[6] Additionally, HANPs have been extensively applied to remediate soils,[9] sediments,[10] groundwater,[11] and nuclear wastewaters[12] contaminated with metals (e.g., Pb, Cd, Cu, and As) and radionuclides (e.g., ^{90}Sr and ^{60}Co), including most effective remediation by encapsulating radionuclide in the apatite mineral structure.[13] As these applications are expected to increase in the future, HANPs will consequently be increasingly introduced into the subsurface environments.

Iron oxides such as goethite and hematite occur ubiquitously in nearly all surficial soils and sediments,[14] and play pivotal roles in the fate, transport, bioavailability, and cycling of P, including HANPs, because they often exhibit a large sorption capacity toward P.[15−17] Especially, naturally occurring goethite nanoparticles (GNPs) have been increasingly demonstrated to determine the bioavailability and cycling of P because of their nanoscale size and high reactivity (i.e., reactive crystal face).[18,19] Consequently, the fate, transport, and cycling of HANPs in the subsurface environments are expected to be, in part, controlled by GNPs. Nonetheless, knowledge of how and to what extent GNPs impact the fate and transport of HANPs in porous media is almost nonexistent. In particular, the mobile GNPs that are generated by remobilization of existing colloids sorbed onto soils and sediments as a result of hydrogeochemical perturbations (e.g., change in pH, ionic strength, and flow rate) of aquifer systems[20] are anticipated to profoundly influence the mobility of HANPs in the subsurface environments, i.e., cotransport of HANPs with mobile GNPs.

pH is often considered to be a key factor in mediating the transport and retention of NPs in porous media.[21−24] The isoelectric point (IEP) of goethite is reached at pH around 7.6−9.4,[25] hence GNPs can be positively or negatively charged

Received: March 9, 2015
Revised: June 16, 2015
Accepted: June 17, 2015
Published: June 17, 2015

DOI: 10.1021/acs.est.5b01210
Environ. Sci. Technol. 2015, 49, 8461−8470

at environmentally relevant pH. Because HANPs exhibit negative surface charge[26] at prevailing pH (6−8),[27] they are expected to strongly sorb onto positively charged GNPs (i.e., heteroaggregation)[28,29] via electrostatic attraction, or remain dispersed when GNPs are negatively charged due to repulsive interaction,[30] both of which will likely influence the cotransport of these two types of NPs in porous media.[24,31] Alternatively, pH is likely to determine the dissolution kinetics of HANPs,[32] which will govern their transport and P provision in plant rhizosphere.[7] Another critical factor that may affect the cotransport of HANPs and GNPs is natural organic matter (NOM),[33] which occurs in all aquatic environments.[34,35] NOM is well-known to influence the transport behaviors of single-species NPs (e.g., HANPs or GNPs alone) in porous media by modifying their surface properties and consequently invoking electrosteric repulsion,[30,31,36] which, in turn, is dependent upon the thickness, mass, and configuration of sorbed NOM layer and NOM type.[34,35,37−39] Therefore, it is anticipated that pH and NOM will strongly affect the cotransport of HANPs and GNPs in porous media.

The overall objective of this research was to unravel the roles of environmentally relevant pHs and NOM types and concentrations on the cotransport and retention of HANPs and GNPs. Our findings provide valuable insights into the coupling interaction between colloidal P and Fe in response to variability in pH and NOM type and concentration.

MATERIALS AND METHODS

HANPs, GNP, and NOM. HANPs (>99.9% purity) were purchased from Nanjing Emperor Nanomaterial Co. Ltd., China. Basic characterizations including primary size and shape, specific surface area (SSA), and elemental composition of the HANPs were conducted previously.[36] Briefly, the HANPs are rod-shaped, 20 nm wide and 100 nm long (i.e., 100 nm in diameter), and have a SSA of 154 m^2 g^{-1} and a Ca/P molar ratio of 1.65. GNPs were synthesized using the method of Schwertmann and Cornell.[17] Briefly, 180 mL of 5 M KOH was rapidly added to 100 mL of 1 M $Fe(NO_3)_3$ while stirring. The mixture was immediately diluted with deionized water to a final volume of 2 L and was then held in a closed polyethylene flask at 70 °C for 60 h. The synthesized GNPs were purified through 10 cycles of deionized water washes, freeze-dried, ground with mortar and pestle, and passed through a No. 70 standard sieve (212 μm opening).

Additional characterizations of the HANPs and detailed characterizations of the GNPs were performed in this study. Briefly, mineral phase identification of HANPs and GNPs was analyzed using the Bruker D8 Advance X-ray diffractometer (Bruker Corp., Billerica, MA). The primary size and shape of GNPs were determined by the JEM-3100 transmission electron microscope (TEM; JEOL, Japan). The SSA of GNPs was measured with the Micromeritics 3000 Surface Area and Porosity Analyzer (Micromeritics Instrument Corp., Norcross, GA). Functional groups of the HANPs and GNPs were recorded using the Thermo Nico Fourier transform infrared (FTIR) spectrometer (Waltham, MA). The IEP of GNPs was examined via the Zetasizer Nano ZS (Malvern Instruments, Southborough, MA). Details on these physicochemical characterizations are given in Supporting Information (SI) S1.

Suwannee River humic acid (SRHA, Standard II) and fulvic acid (SRFA, Standard I) were purchased from the International Humic Substances Society (St. Paul, MN). These model NOM compounds have been used as analogues for natural environments.[40−42] The preparation and characterization of SRHA and SRFA stock solutions are provided in SI S2.

Porous Media. Quartz sand (Accusand C-190, Unimin Corp., Le Sueur, MN) served as model granular porous media. The manufacturer reported that median grain size (d_{50}) of the sand was 688 μm and the uniformity coefficient ($U_i = d_{60}/d_{10}$, where d_x represents the grain diameter at x% mass passing[43]) was 1.13. Prior to use, the sand was cleaned using a sequential acid−base deionized water wash procedure. Surface morphological features of the cleaned sand were observed using the JSM-7400F scanning electron microscope (SEM, JEOL) (see SI Figure S1). The particles from pulverized quartz sand were used as surrogates for the sand and for electrophoretic mobility (EM) measurements using the Zetasizer Nano ZS.

Preparation and Characterization of HANPs−GNPs Influent Suspensions. The GNPs stock suspension was first generated by suspending 0.200 g of GNPs dry powder in 1 L of deionized water, sonicating for 1 h to disperse particles, and then centrifuging the suspension at 100g for 2 min to remove large aggregated particles (>2 μm) based upon the Stokes' law. The concentration of resulting GNPs stock suspension was quantified using the UV−vis spectrophotometer (DU Series 640, Beckman Instruments Inc., Fullerton, CA) at the wavelength of 390 nm (see SI S3 and Figure S2) and was ∼150 mg L^{-1}. The HANPs−GNPs influent suspension was then prepared by adding HANPs dry powder to a predetermined volume of GNPs stock suspension, and diluting the suspension with KNO_3 solution (background electrolyte) to obtain HANPs, GNPs, and KNO_3 concentrations of 200 mg L^{-1}, 100 mg L^{-1}, and 0.1 mM, respectively. Because the ultimate goal of this research is to extend our understanding of application of HANPs as a promising P nanofertilizer and an in situ amendment for contaminated site remediation, a high concentration of 200 mg L^{-1} was chosen for the HANPs, which is similar to those commonly used in nanofertilizer application (∼120 mg L^{-1} HANPs)[6] and in contaminated site remediation particles (200 mg L^{-1} HANPs).[9] Additionally, an environmentally relevant concentration of 100 mg L^{-1} was chosen for the GNPs,[20] consistent with those for transport of iron oxide colloids (30−111 mg L^{-1} hematite) in porous media.[44,45] Recent studies demonstrated that the concentration ratio between negatively and positively charged NPs (e.g., silver and hematite NPs, and carbon nanotube and hematite NPs)[29,46] played an appreciable role in their heteroaggregation. The concentration ratio of HANPs/GNPs (2:1) used is consistent with those (0.4−13) employed in NP heteroaggregation studies.[29,46] The pH of HANPs−GNPs influents was adjusted to 6.5, 7.5, and 10.5 using 1 mM HNO_3 or NaOH (Table 1). To elucidate the effects of NOM type and concentration on the cotransport of HANPs and GNPs, HANPs−GNPs influents were prepared with SRHA/SRFA stock solution to yield environmentally relevant concentrations (0, 0.1, 1, and 10 mg L^{-1})[34,35] of SRHA/SRFA (Table 1). The pH of HANPs−GNPs influents in the presence of NOM was unadjusted and was ∼7.5.

TEM was employed to unravel the interaction (e.g., heteroaggregation) between HANPs and GNPs at selected solution chemistries. The EM and average hydrodynamic diameter (D_H) of HANPs−GNPs influents at the desired solution chemistries were analyzed using the Zetasizer Nano ZS and dynamic light scattering (DLS; Möbiuζ, Wyatt Technology Corp., Santa Barbara, CA), respectively. The refractive index of water (1.33) was employed during DLS measurements. The

DOI: 10.1021/acs.est.5b01210
Environ. Sci. Technol. 2015, 49, 8461−8470

Table 1. Mass Balance Percentages and Fitted Parameters of the One-Site Kinetic Retention Model for the Cotransport of HANPs and GNPs in Saturated Packed Column Experiments at Varying pHs and NOM Concentrations and Types[a]

				HANPs							GNPs						
				(%)							(%)						
pH	SRHA (mg L^{-1})	SRFA (mg L^{-1})	n	M_{eff}	M_{ret}	M_{tot}	S_{max}/C_0 (cm^3 g^{-1})	k_r (min^{-1})	β	R^2	M_{eff}	M_{ret}	M_{tot}	S_{max}/C_0 (cm^3 g^{-1})	k_r (min^{-1})	β	R^2
6.5			1	23.6	59.6	83.2	8.00	1.64	0.432	0.905	3.55	104	108	8.07	4.70	0.432	0.993
7.5			2	5.52	90.5	96.0	10.5	2.56	0.432	0.998	4.02	98.9	103	8.00	1.97	0.432	0.971
10.5			2	90.6	10.5	101	0.114	0.927	0.432	0.928	83.7	8.29	92.0	0.142	0.601	0.432	0.942
7.6	0.1		1	58.5	33.3	91.8	15.0	7.16	1.35	0.934	66.4	34.3	101	1.31	33.1	1.57	0.959
7.6	1		2	86.5	5.24	91.7	0.120	16.9	1.20	0.942	93.9	2.46	96.4	6.65×10^{-2}	20.8	1.11	0.962
7.6	10		2	97.1	3.46	101	7.53×10^{-2}	34.3	1.12	0.947	100	1.87	102	6.61×10^{-2}	6.56	0.709	0.944
7.7		0.1	1	68.7	23.3	92.0	13.3	14.0	1.85	0.933	72.4	14.3	86.7	0.289	30.5	1.35	0.889
7.7		1	2	86.4	8.12	94.5	0.158	22.4	1.36	0.938	93.9	3.32	97.2	7.56×10^{-2}	10.3	0.861	0.936
7.7		10	2	87.7	6.44	94.1	0.134	18.8	1.28	0.933	98.8	2.64	101	5.96×10^{-2}	7.98	0.810	0.966

[a] n, replicate column experiments; M_{eff}, M_{ret}, and M_{tot} are effluent, retentate, and total percentages of NPs recovered from column experiments, respectively (mean values are reported); S_{max}/C_0, normalized maximum solid-phase concentration of retentates; k_r, first-order retention rate coefficient; β, an empirical parameter controlling the shape of spatial distribution for retentates; and R^2, squared Pearson's correlation coefficient, estimated from the one-site kinetic retention model.

EM and D_H information was used in combination with extended Derjaguin–Landau–Verwey–Overbeek (XDLVO) theory to calculate the interaction energy between NPs and sand grains (see SI S4).

Column Experiments. Column experiments were conducted following procedures described previously.[36] Briefly, a glass chromatography column (1.7 cm i.d. × 10 cm long) was dry packed with 31.4 g of the cleaned sand, yielding a bulk density of 1.38 g cm^{-3}. Afterward, >20 pore volumes (PVs) of deionized water were introduced in an upflow mode at a Darcy velocity of 0.441 cm min^{-1} to saturate the column. The gravimetrically measured porosity of the packed column was ~0.3.

Following the saturating step, a nonreactive tracer (50 mM KNO_3) test was performed to assess hydrodynamic properties of the column (Peclet number and hydrodynamic dispersion coefficient of ~99 and 0.045 cm^2 min^{-1}, respectively) by fitting the tracer breakthrough curve (BTC) to one-dimensional advection–dispersion equation. After the tracer test, >20 PVs of background electrolyte solution (0.1 mM KNO_3) were injected into the column to equilibrate pore-water solution chemistry. Five PVs of the HANPs–GNPs influent suspension under different pHs or SRHA/SRFA concentrations (Table 1) were introduced in the column, followed by elution with 5 PVs of NP-free background electrolyte solution. During the cotransport experiments, the HANPs–GNPs influent was periodically sonicated to avoid NPs settlement and maintain suspension stability. The velocity for all cotransport experiments including tracer tests was set to 0.441 cm min^{-1} to represent typical fluid velocities in coarse aquifer sediments[47] or forced-gradient conditions (e.g., in situ groundwater remediation).[48]

Effluent samples were collected continuously using a fraction collector (Foxy Jr., Teledyne Isco, Lincoln, NE). Following completion of each cotransport experiment, the retained HANPs and GNPs (hereafter designated as retentate) were determined. The end fitting of the column was removed and the sand grains were carefully excavated in 1-cm increments (10 layers for a column) into 50-mL centrifuge tubes. Excess eluant solution (deionized water or 1 mM NaOH, depending on suspension pH) was added to the centrifuge tube. The tube was shaken at a low speed of 50 rpm for 1 h (this equilibrium time interval was chosen to be consistent with the duration of the cotransport experiments) and then sonicated at a low frequency of 20 kHz[49] for 30 min to liberate the retained HANPs and GNPs. This gentle liberation procedure was employed here to avoid introducing any undesirable artifacts that might alter the size distributions of the retentates (e.g., induced by being vigorously shaken or sonicated at a high frequency). Additionally, the D_H of the retentates was controlled to be completed within 2 h to avoid potential interference from NP reaggregation. The concentrations of phosphate in the effluents and retentates were quantified using the phosphomolybdate blue method,[50] whereas the concentrations of GNPs in these samples were determined spectrophotometrically at the wavelength of 390 nm (described above). The measured phosphate concentrations were then used to calculate the concentrations of HANPs in the effluents and retentates. The pH of column influents and effluents was found to remain constant (ΔpH ≤0.3) during the course of experiments.

To better understand the mechanisms controlling the cotransport of HANPs and GNPs in saturated sand, batch experiments were performed to explore the dissolution of

DOI: 10.1021/acs.est.5b01210
Environ. Sci. Technol. 2015, 49, 8461–8470

Table 2. Average Hydrodynamic Diameters (D_H) of HANPs−GNPs Samples in the Influents, Effluents, and Retentates in the Column at Different Depths Under Different pHs and NOM Concentrations and Types[a]

			D_H of HANPs−GNPs samples (nm)						D_H of individual NPs (nm)	
					retentate (cm)					
pH	SRHA (mg L^{-1})	SRFA (mg L^{-1})	influent	effluent	0−1	1−2	2−3	D_H/d_{50}	HANPs	GNPs
6.5			2835 ± 677 a	984 ± 183 a	3196 ± 529 a	1836 ± 173 b	731 ± 70 a	4.6×10^{-3}	1021 ± 192 a	632 ± 24 a
7.5			1656 ± 117 b	810 ± 171 a	2215 ± 378 b	2404 ± 206 a	834 ± 67 a	3.5×10^{-3}	907 ± 80 b	626 ± 28 a
10.5			401 ± 16 c	325 ± 22 b	658 ± 195 c	445 ± 240 c	585 ± 12 b	9.6×10^{-4}	274 ± 12 c	310 ± 15 b
7.6	0.1		387 ± 15 c	359 ± 10 b	483 ± 67 c	356 ± 71 b	421 ± 78 b	7.0×10^{-4}	375 ± 48 c	363 ± 24 b
7.6	1		282 ± 5.9 d	264 ± 7.1 b	458 ± 93 c	348 ± 63 b	352 ± 98 b	6.7×10^{-4}	272 ± 14 d	268 ± 16 c
7.6	10		282 ± 7.6 d	257 ± 7.1 b	362 ± 74 c	361 ± 47 b	351 ± 56 b	5.3×10^{-4}	224 ± 36 e	213 ± 11 d
7.7		0.1	472 ± 20 c	395 ± 8.8 b	574 ± 205 c	565 ± 129 b	448 ± 217 b	8.3×10^{-4}	391 ± 17 c	373 ± 20 b
7.7		1	293 ± 4.9 d	290 ± 4.1 b	411 ± 81 c	400 ± 52 b	383 ± 19 b	6.0×10^{-4}	257 ± 27 d	247 ± 13 c
7.7		10	287 ± 4.0 d	273 ± 4.4 b	385 ± 41 c	369 ± 80 b	331 ± 70 b	5.6×10^{-4}	246 ± 19 d	234 ± 12 c

[a] d_{50} is the median grain size of collector. Maximum D_H/d_{50} values are reported to test the physical straining (here the D_H is average hydrodynamic diameter of HANPs−GNPs sample). The D_H of individual HANPs and GNPs is also reported for comparison. Mean values ± standard deviations in each vertical column followed by the same lowercase letters are not significantly different using Tukey's HSD test at $p < 0.05$.

HANPs as a function of pH without/with GNPs copresent in the suspension over the time frame of the cotransport experiments (~1.1 h), which is given in SI S5. Furthermore, the D_H of HANPs−GNPs in the effluents and retentates near the column inlet (0−1, 1−2, and 2−3 cm) was examined. Additionally, some solid-phase samples close to the column inlet (0−1 cm) were collected and prepared for SEM energy-dispersive X-ray analysis using the Zeiss Auriga 60 High Resolution Focused Ion Beam & SEM Crossbeam workstation (Carl Zeiss Microscopy GmbH, Jena, Germany).

Data Analysis. A one-dimensional form of the advection−dispersion equation with one kinetic retention site was used to simulate the transport and retention of HANPs and GNPs, respectively, under different pHs and NOM concentrations (see SI S6). Additionally, one-way ANOVA analysis was performed to identify statistical differences in measured parameters using the Tukey's Honestly Significant Different (HSD) test. All statistical analyses were performed using SPSS 16.0 and the differences of means were considered significant at $p < 0.05$.

RESULTS AND DISCUSSION

Characterization of HANPs and GNPs. HANPs and GNPs were found to be single-phase pure hydroxyapatite (PDF 01-074-9761) and goethite (PDF 00-017-0536) minerals (SI Figure S3). TEM images show that the GNPs are acicular crystals 90 nm wide and 1850 nm long (SI Figure S4a, b). Selected-area electron diffraction pattern of the GNPs displayed *d*-spacing of 1.34, 1.55, and 3.20 Å (SI Figure S4c), consistent with the reported results for goethite.[19,41] The SSA of GNPs is 122.4 $m^2\ g^{-1}$, which is comparable to the documented values (9−153 $m^2\ g^{-1}$).[51,52] For HANPs, three characteristic bands at 960, 1030, and 1092 cm^{-1} are assigned to PO_4^{3-} stretching vibrations,[53] whereas the two characteristic peaks at 795 and 897 cm^{-1} belong to Fe−O stretching vibrations of GNPs (SI Figure S5).[17] The IEP of GNPs was determined to be around pH 7.9 (SI Figure S6), consistent with reported results (7.6−9.4).[25]

Electrophoretic Mobility and Average Hydrodynamic Diameters of HANPs−GNPs Influents. The EM and D_H of HANPs−GNPs influents at varying pHs and NOM concentrations are summarized in SI Table S1 and Table 2, respectively. Our measurements indicate that the HANPs−GNPs influents were negatively charged over the range of solution chemistries investigated. The EM increased with increasing pH especially when the pH (10.5) was above IEP_{GNPs} (SI Figure S6b) likely due to deprotonation of HANPs[54] and GNPs.[55] Similar findings have been well-documented by Elimelech et al.[30] At the lowest pH of 6.5 (<IEP_{GNPs}), the HANPs−GNPs influent was still negatively charged, possibly because the EM absolute value of negatively charged HANPs ($-1.61 \times 10^{-8}\ m^2\ s^{-1}\ V^{-1}$) was greater than that of positively charged GNPs ($+1.40 \times 10^{-8}\ m^2\ s^{-1}\ V^{-1}$) (SI Figure S6). For the HANPs−GNPs influents containing NOM, their EMs became significantly ($p > 0.05$) more negative with increasing NOM concentration, mainly due to enhanced sorption of NOM (primarily the carboxylic and phenolic functional groups) onto HANPs and/or GNPs through van der Waals, hydrogen bonding, dipole−dipole, hydrophobic, and/or ligand exchange interactions.[34,35,38,39,41,55,56] Furthermore, their EMs were more negative in the presence of SRHA relative to SRFA because the SRHA exhibits a stronger affinity toward NPs (e.g., C_{60})[57,58] due to its higher molecular weight and charge density and smaller aromatic backbone than the SRFA.[34,38,40,41,56]

The D_H values of HANPs−GNPs influents increased significantly ($p < 0.05$) with decreasing pH (Table 2), likely due to greater homoaggregation of HANPs and GNPs, and/or heteroaggregation between HANPs and GNPs. TEM images of the HANPs−GNPs influent (Figure 1) at pH 7.5 indicate that homoaggregation of both HANPs and GNPs was apparent. Particularly, the negatively charged HANPs were found to sorb onto positively charged GNPs, forming large HANPs−GNPs

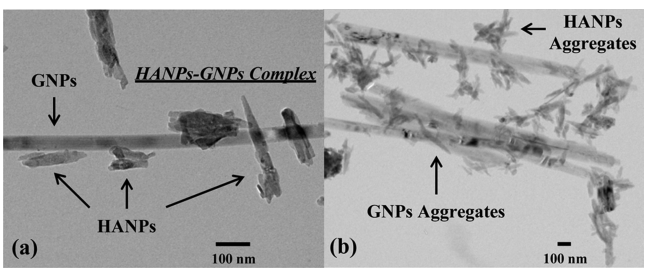

Figure 1. TEM images of HANPs−GNPs influent at pH 7.5. Scale bar in panels a and b is 100 nm.

DOI: 10.1021/acs.est.5b01210
Environ. Sci. Technol. 2015, 49, 8461−8470

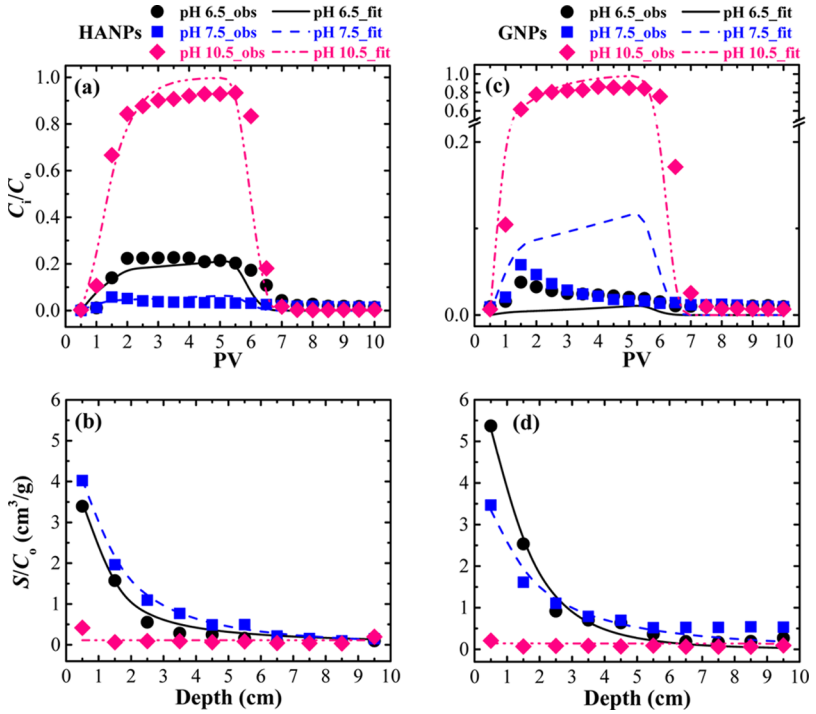

Figure 2. Measured (symbols) and fitted (lines) cotransport breakthrough curves (a, c) and retention profiles (b, d) of HANPs (a, b) and GNPs (c, d), respectively, under pHs 6.5, 7.5, and 10.5 in saturated sand columns when median grain size of 688 μm and Darcy velocity of 0.441 cm min^{-1}. Fitted curves in (a–d) were obtained using the one-site kinetic retention model. In b and d the normalized concentrations (mass of the HANPs/GNPs recovered in the sand (S) divided by C_0) are plotted with distance from the column inlet.

complexes. Similar results were recently reported for the heteroaggregation between negatively charged carbon nanotubes and positively charged hematite NPs.[29] As anticipated, the D_H values of HANPs–GNPs influents decreased significantly ($p < 0.05$) with increasing NOM concentration, and the SRHA was more effective than the SRFA in suppressing HANPs–GNPs aggregation, consistent with their EM trends and published results.[29,30,37,57,58]

Effect of pH on the Cotransport of HANPs and GNPs. Measured and fitted BTCs and retention profiles (RPs) of HANPs and GNPs at varying pHs (6.5, 7.5, and 10.5) in saturated sand columns are presented in Figure 2. The BTCs are plotted as normalized effluent concentrations (C_i/C_0) versus PVs, and the RPs are plotted as normalized solid-phase concentrations (S/C_0) with distance from the column inlet. A high degree of confidence in our experimental results is attested from high mass recoveries for both HANPs (83.2–101%) and GNPs (86.7–108%), as well as low standard deviations (≤4.3%) between two replicate column experiments ($n = 2$) (Table 1).

In the following we first discuss the transport and retention of GNPs under different pHs since the HANPs are likely to dissolve at low pH,[32] which may perplex the mechanism explanation for HANPs. Total effluent recovery (M_{eff}) of GNPs increased from 3.55 to 4.02, and considerably to 83.7% when the pH was increased from 6.5 to 7.5, and to 10.5, respectively (Figure 2c and Table 1). Intriguingly, the BTCs of GNPs evolved from ripening (increasing retention rate with time) to blocking (decreasing retention rate with time) behaviors with increasing pH. Specifically, when pH (6.5 and 7.5) < IEP_{GNPs} the ripening BTC was encountered, whereas the blocking BTC occurred at pH (10.5) > IEP_{GNPs} (Figure 2c). A similar transition from ripening to blocking phenomena was reported for the transport of colloids (e.g., latex)[59] and NPs (e.g., TiO_2)[60] with decreasing electrolyte concentration in saturated sand columns. This is primarily due to the distinct size differences among HANPs–GNPs influents at varying pHs (Table 2). At low pHs of 6.5 and 7.5, the D_H values of HANPs–GNPs influents were as high as several μm, and interception and sedimentation are expected to play appreciable roles in the retention of GNPs during transport in porous media based on the classical filtration theory (CFT)[61] and more quantitatively on the Tufenkji–Elimelech equation,[62] which predicts that the interception and sedimentation efficiencies increase with increasing D_H (1–10 μm). Additionally, low electrostatic repulsion between particle and sand grain may partly contribute to the low mobility of GNPs at low pHs (SI Table S1 and Figure S7a). Particularly, the values of primary energy barriers (Φ_{max}) between particle–sand systems were <0 at pHs 6.5 and 7.5, indicative of favorable attachment conditions. Cai et al.[24] also observed that the transport of positively charged TiO_2 NPs was limited ($M_{eff} \approx 10\%$) in the copresence of negatively charged C_{60} NPs under favorable attachment conditions. In contrast with CFT[61] that predicts exponential profile with depth, the RPs of GNPs exhibited a hyperexponential profile with greater retention near the column inlet (0–3 cm) and rapidly decreasing retention with depth (Figure 2d). The hyperexponential RPs became more pronounced at lower pHs. Consistent with previous findings,[63,64] physical straining may contribute to the ripening BTCs and hyperexponential RPs of GNPs at low pHs since the maximum values of D_H/d_{50} (4.6×10^{-3} and 3.5×10^{-3}, respectively, at pHs 6.5 and 7.5, Table 2) were greater than the threshold value for straining (0.002).[43]

The greatest mobility of HANPs was found to occur at pH 10.5 (Figure 2a, b), consistent with the results of GNPs under

DOI: 10.1021/acs.est.5b01210
Environ. Sci. Technol. 2015, 49, 8461–8470

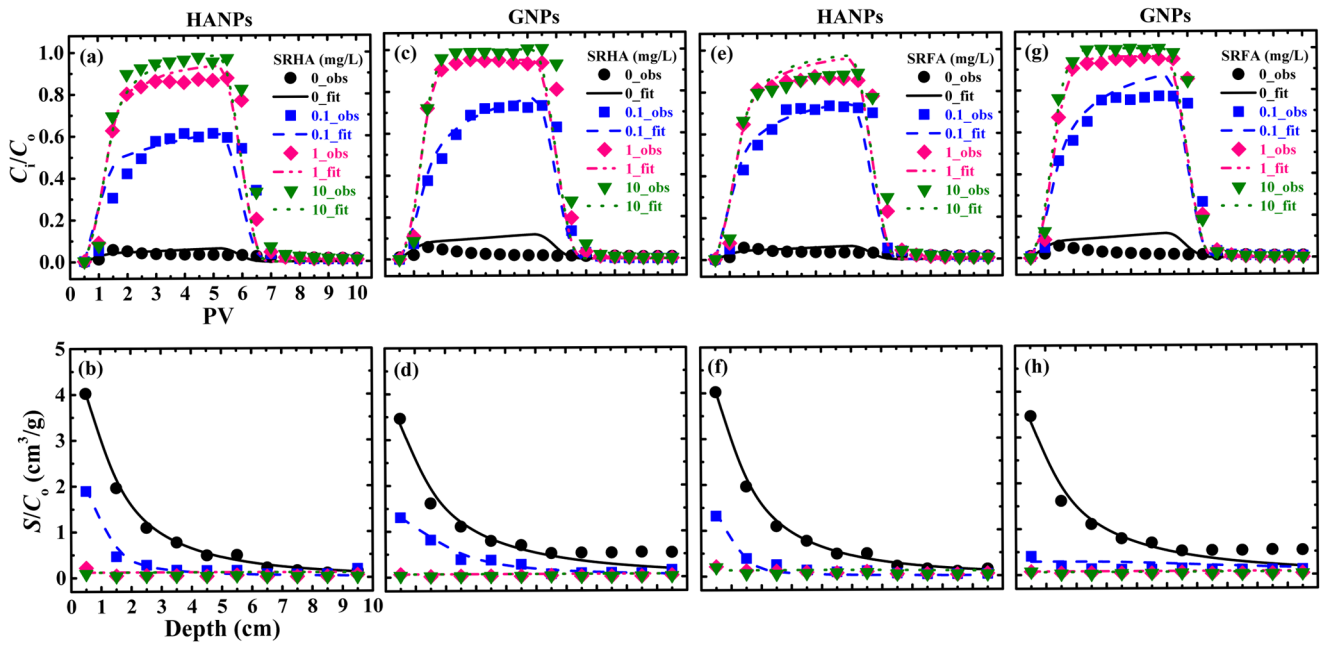

Figure 3. Measured (symbols) and fitted (lines) cotransport breakthrough curves (a, c, e, and g) and retention profiles (b, d, f, and h) of HANPs (a, b, e, and f) and GNPs (c, d, g, and h), respectively, under different concentrations (0, 0.1, 1, and 10 mg L^{-1}) of SRHA (a–d) and SRFA (e–h) in saturated sand columns when median grain size of 688 μm and Darcy velocity of 0.441 cm min^{-1}. Fitted curves in (a–h) were obtained using the one-site kinetic retention model.

different pHs (Figure 2c, d). In addition to the roles of influent size difference, electrostatic interaction, and straining described above, another explanation for this result is that the overall favorable retention sites (e.g., metal oxide impurities) on collector surfaces decrease with increasing pH due to deprotonation of these favorable sites.[65] However, the mobility of HANPs was much greater at pH 6.5 than at pH 7.5 (M_{eff} = 23.6% vs 5.52%, Figure 2a, b and Table 1), which was inconsistent with the trends for GNPs. The dissolution of HANPs in HANPs–GNPs suspensions versus pH over the time frame of cotransport experiments (1.1 h) in batch experiments shows that negligible dissolution of HANPs occurred when pH ≥7.5, whereas 9.8% HANPs were dissolved at pH 6.5 (SI Figure S8). The mobility of dissolved PO_4^{3-} ion was much greater than those of aggregated HANPs (Figure 1) and HANPs–GNPs complexes (Figure 1 and SI Figure S9), thereby contributing to the enhanced transport of HANPs (including PO_4^{3-} ions) at pH 6.5. Nonetheless, the limited dissolution (9.8%) of HANPs at pH 6.5 in batch system cannot fully explain the high mobility of HANPs (M_{eff} = 23.6%) in column system. Potential mechanisms are discussed below: (i) the dissolution of HANPs could be much higher in "dynamic" column system than that in "static" batch system particularly when injecting pH 6.5 background electrolyte solutions to elute (and dissolve) previously retained HANPs and/or HANPs–GNPs complexes, since the dissolved PO_4^{3-} ions were continuously eluted out from the column, and (ii) the rate and extent of dissolution for HANPs depends on time,[32] and the dissolved PO_4^{3-} ion could be resorbed onto positively charged GNPs during cotransport, which, in turn, influences the cotransport of HANPs and GNPs. Indeed, at 1.1 h, roughly 1.4% of the dissolved PO_4^{3-} ions was resorbed onto the GNPs at pH 6.5 in batch system (SI Figure S8). Therefore, heteroaggregation between negatively charged HANPs (SI Figure S6a) and positively charged GNPs (SI Figure S6b) is progressively weakened during cotransport due to a decrease in electrostatic attraction (i.e., GNPs become less positively charged with PO_4^{3-} sorption). Consequently, enhanced dissolution of HANPs in "dynamic" column system, resorption of dissolved PO_4^{3-} ions onto GNPs, and reduced heteroaggregation between HANPs and GNPs are likely to contribute to the high mobility of HANPs (including PO_4^{3-} ions) at pH 6.5.

In comparing the cotransport of HANPs and GNPs with individual transport of HANPs (or GNPs), the mobility of HANPs (or GNPs) in the copresence of GNPs (or HANPs) was greater than that without GNPs (or HANPs) at pH 10.5 (SI Figure S10). This is likely because the negatively charged HANPs compete with negatively charged GNPs for favorable retention sites on the collector surfaces, contributing to increased transport and blocking BTCs for both HANPs and GNPs.[24] However, the opposite trends were obtained for both NPs at a low pH of 7.5 (SI Figure S11), likely ascribed to the fact that heteroaggregation (Figure 1) between negatively charged HANPs and positively charged GNPs determines the cotransport of HANPs and GNPs. This finding also underlines that influent particle size is an indicator of mobility for NPs in porous media (SI Figure S11).

The particle size distribution of HANPs–GNPs samples in the influents, effluents, and retentates under different pHs is shown in Table 2. Always, the D_H values of HANPs–GNPs samples followed the order of retentate (0–1 cm) > influent > effluent. Furthermore, the D_H differences among these three reservoirs became smaller with increasing pH. Additionally, for the retentates, their D_H values decreased as the transport distance increased, i.e., from 0–1 to 2–3 cm, with the exception of the one from 1–2 to 2–3 cm at pH 10.5. These observations indicate that large HANPs–GNPs aggregates were more efficiently removed during cotransport, i.e., larger HANPs–GNPs preferentially retained near the column inlet (which was partly substantiated in SI Figure S12) and smaller ones eluted out, thereby developing the size-selective retention.[36,61] This

DOI: 10.1021/acs.est.5b01210
Environ. Sci. Technol. 2015, 49, 8461–8470

could be due to the greater degrees of ripening (Figure 2) and straining (Table 2), enhanced heteroaggregation of influents (Table 2), and higher collision efficiency due to interception and sedimentation because of a larger effective particle size (Table 2 and SI Figure S12), or more likely to a combination of these factors.[61,62] Similar results were reported for the transport of individual types of NP (e.g., HANPs,[36] carbon nanotubes,[66] or ZnO[63]) in porous media. Please note that even at pH 10.5 where repulsive interaction predominates (SI Figure S7a), the size-selective retention nevertheless occurred likely due to homoaggregation of HANPs and GNPs during cotransport.

The one-site kinetic retention model well-approximated the BTCs and RPs of both NPs at varying pHs with the exception of GNPs BTCs at pHs 6.5 and 7.5, because the model did not account for ripening effect (Figure 2 and Table 1). Although a ripening model that incorporates attractive particle−particle interaction can capture the main feature of the ripening BTCs,[64] the ripening model was not used in this study since the blocking BTCs were encountered under most solution chemistries employed (see below). Nevertheless, the model-fitted parameters from the one-site kinetic retention model still provide useful insight. For both NPs, the values of retention rate coefficient (k_r), especially normalized maximum solid-phase concentration of retentates (S_{max}/C_0), at pH 10.5 were significantly smaller than those obtained at low pH (i.e., pH 6.5). These results suggest that mechanisms controlling NPs cotransport and retention particularly near the column inlet were controlled by pH. Specifically, larger values of S_{max}/C_0 tended to produce more marked hyperexponential RPs (Figure 2b, d).[67,68] However, the trends of k_r and S_{max}/C_0 for HANPs were inconsistent with those of GNPs at pHs 6.5 and 7.5, most likely influenced by the dissolution of HANPs at pH 6.5 (SI Figure S8).

Effects of NOM Concentration and Type on the Cotransport of HANPs and GNPs. The NOM concentration and type were found to have a marked influence on the cotransport and retention of HANPs and GNPs (Figure 3). Regardless of NOM type, the transport of both NPs increased with increasing NOM concentration. For example, the M_{eff} values of HANPs and GNPs increased from 5.52 to 97.10% and from 4.02 to 100%, respectively, when SRHA concentration was increased from 0 to 10 mg L^{-1} (Table 1). A similar trend of increasing M_{eff} value was achieved for both NPs with increasing SRFA concentration (Table 1). This is largely due to less aggregation of NPs (Table 2) and greater electrosteric repulsion between NP−sand systems at higher NOM concentrations (SI Table S1 and Figure S7b, c). Moreover, the SRHA was more effective than the SRFA in elevating NPs mobility at high NOM concentrations, i.e., 1 and 10 mg L^{-1} (Figure 3 and Table 1), likely attributed to reduced aggregation of NPs (Table 2) and enhanced electrosteric repulsion between NPs and sand grains in the presence of SRHA relative to SRFA (SI Table S1). Similar findings have been reported for the transport of one type of NP individually in porous media.[36,42,57,58]

Irrespective of NOM concentration and type, the mobility of HANPs was always lower than that of GNPs (Figure 3 and Table 1). For instance, 58.5% of the injected HANPs broke through when SRHA = 0.1 mg L^{-1}, whereas the value was 66.4% for GNPs. This is likely because at pH 7.6, the negatively charged NOM exhibits a lower affinity toward the negatively charged HANPs (SI Figure S6a) than to the positively charged GNPs (SI Figure S6b),[55,56] thus resulting in less electrosteric repulsion to HANPs compared to GNPs. The D_H of individual HANPs was always larger than that of individual GNPs at a specific NOM concentration (Table 2), supporting that the NOM stabilizes GNPs to a greater extent than HANPs due to greater electrosteric repulsion. These findings again reflect that the D_H of NPs is an indicator of their mobility in porous media (as discussed at different pHs). Consistent with the results obtained at pH 10.5 (Figure 2), the blocking BTCs of both NPs occurred in the presence of NOM even at NOM concentration as low as 0.1 mg L^{-1} (Figure 3a, c, e, and g), implying that NOM effectively stabilizes HANPs, GNPs, and/or HANPs−GNPs complexes by invoking electrosteric repulsion. Indeed, the Φ_{max} value between NP−sand systems increased considerably from <0 to 297 kT and from <0 to 229 kT (where k is the Boltzmann constant and T is the absolute temperature), respectively, when SRHA and SRFA concentration was increased from 0 to 10 mg L^{-1} (SI Table S1). Additionally, the blocking BTCs became less significant with elevating NOM concentration (Figure 3a, c, e, and f) likely because NOM acts to mask the favorable retention sites of collector. Pretreatment of the column with 10 mg L^{-1} SRHA resulted in a higher mobility of both NPs under 10 mg L^{-1} SRHA relative to those in the untreated columns (SI Figure S13), confirming that NOM masks the favorable retention sites of porous media. These findings are in good agreement with those elaborated by Tufenkji and Elimelech.[65] Regarding the RPs for both NPs, their shapes generally transformed from hyperexponential to flat with increasing NOM concentration, again because of reduced aggregation of NPs and enhanced electrosteric repulsion between NP−sand systems. The flat RPs obtained at 10 mg L^{-1} SRHA/SRFA were likely attributed to the fact that high concentration of NOM masks most of these favorable retention sites of the collector (SI Figure S13). However, careful examination of D_H values for HANPs−GNPs samples in the influents, effluents, and retentates again indicates that the size-selective retention occurred even at NOM concentration as high as 10 mg L^{-1} (Table 2). This could be due to homoaggregation of HANPs and GNPs (SI Figure S14) and/or heteroaggregation of HANPs−GNPs complexes (Figure 1).

The one-site kinetic retention model again well-described the BTCs and RPs of both NPs in the presence of NOM (Figure 3 and Table 1). The values of S_{max}/C_0 decreased with increasing NOM concentration, signifying that mechanisms governing NPs cotransport and retention were highly controlled by the maximum retention sites. Additionally, the values of β also decreased with increasing NOM concentration. A higher value of β reflects a stronger depth-dependent retention near the column inlet, which commonly yields the hyperexponential RPs (Figure 3).[67,69] Nonetheless, the values of k_r for HANPs exhibited inconsistent trend in response to variability in NOM concentration, further reflecting that the transport and retention kinetics of HANPs was predominated by the S_{max}/C_0.

Environmental Implications. This research provides valuable insights into the application of HANPs as a promising P nanofertilizer and an in situ amendment for contaminated site remediation. With HANPs being a novel P nanofertilizer, we would anticipate minimal eutrophication risks due to their limited mobility (low leaching rate[6−8]) in soils at slightly alkaline pH (pH 7.5), where substantial amounts of positively charged iron oxides are present. Nonetheless, acidic pH conditions (pH ≤6.5) promote the dissolution of HANPs and hence enhance their mobility including dissolved PO_4^{3-} ions. This is of particular interest since plant roots and/or

DOI: 10.1021/acs.est.5b01210
Environ. Sci. Technol. 2015, 49, 8461−8470

associated fungi can produce low-molecular-weight organic acids (e.g., acetate, oxalate, and citrate)[70] in the rhizosphere that may solubilize HANPs and expedite their transport and subsequent uptake by plants. As an in situ amendment, the mobility of HANPs in contaminated sites may be limited because of favorable electrostatic attraction between HANPs and iron oxides. However, the presence of a minute amount of NOM (0.1 mg L^{-1}) can significantly enhance the transport of HANPs through electrosteric repulsion. Furthermore, highly alkaline conditions (pH ≥10.5) also increase the mobility of HANPs due to charge reversal of iron oxides. Therefore, the in situ remediation efficiency of HANPs for contaminated sites is expected to be largely controlled by the coupled interplay among HANPs, iron oxides, and NOM at different pHs.

Widespread application of engineered NPs will result in their dissemination in the subsurface environments, where certain amounts of iron oxides occur as mobile colloids. Our findings indicate that cotransport behaviors of HANPs with GNPs are more complicated than those of their individual transport in porous media, primarily because the transport and retention kinetics of engineered NPs are highly influenced by mobile colloids (e.g., homo- and heteroaggregation, and co- and competitive-retention), and vice versa. To achieve a more complete understanding of the cotransport of engineered NPs with naturally occurring colloids, future study is needed to unravel the roles of other critical factors such as environmentally relevant ionic strengths and flow rates, which are known to impact the individual transport of colloids/NPs.

■ ASSOCIATED CONTENT

Supporting Information

Additional information including characterization of HANPs and GNPs, preparation of NOM stock solution, XDLVO theory, dissolution of HANPs, transport model, Table S1, and Figures S1−S14. The Supporting Information is available free of charge on the ACS Publications website at DOI: 10.1021/acs.est.5b01210.

■ AUTHOR INFORMATION

Corresponding Authors

*E-mail: yjin@udel.edu; tel.: (302)-831-6962; fax: 302-831-0605.

*E-mail: jaisi@udel.edu; tel.: (302)-831-1376; fax: 302-831-0605.

Notes

The authors declare no competing financial interest.

■ ACKNOWLEDGMENTS

This work was supported by research grants from the U.S. Department of Agriculture (NIFA Awards 2012-67019-19320 and 2013-67019-21373). We acknowledge the Advanced Materials Characterization Lab, University of Delaware, for providing XRD, BET, FTIR, and DLS analyses of HANPs and GNPs. Comments and suggestions from four anonymous reviewers and Associate Editor Dr. Daniel Giammar helped us improve the quality this paper.

■ REFERENCES

(1) Cordell, D.; Drangert, J. O.; White, S. The story of phosphorus: Global food security and food for thought. *Global Environ. Change* **2009**, *19* (2), 292−305.

(2) Mackenzie, F. T.; De Carlo, E. H.; Lerman, A. Coupled C, N, P, and O biogeochemical cycling at the land-ocean interface. In Wolanski, E., McClusky, D. S., Eds.; *Treatise on Estuarine and Coastal Science*; Academic Press: Waltham, MA, 2011; Vol 5, pp 317−342.

(3) Conley, D. J.; Paerl, H. W.; Howarth, R. W.; Boesch, D. F.; Seitzinger, S. P.; Havens, K. E.; Lancelot, C.; Likens, G. E. Controlling eutrophication: Nitrogen and phosphorus. *Science* **2009**, *323* (5917), 1014−1015.

(4) Elser, J.; Bennett, E. Phosphorus cycle: A broken biogeochemical cycle. *Nature* **2011**, *478*, 29−31.

(5) Sharpley, A.; Jarvie, H. P.; Buda, A.; May, L.; Spears, B.; Kleinman, P. Phosphorus legacy: Overcoming the effects of past management practices to mitigate future water quality impairment. *J. Environ. Qual.* **2013**, *42* (5), 1308−1326.

(6) Liu, R.; Lal, R. Synthetic apatite nanoparticles as a phosphorus fertilizer for soybean (*Glycine max*). *Sci. Rep.* **2014**, *4*, DOI:10.1038/srep05686.

(7) Montalvo, D.; McLaughlin, M. J.; Degryse, F. Efficacy of hydroxyapatite nanoparticles as phosphorus fertilizer in andisols and oxisols. *Soil Sci. Soc. Am. J.* **2015**, *79* (2), 551−558.

(8) Liu, R.; Lal, R. Potentials of engineered nanoparticles as fertilizers for increasing agronomic productions. *Sci. Total Environ.* **2015**, *514*, 131−139.

(9) Chen, J. H.; Wang, Y. J.; Zhou, D. M.; Cui, Y. X.; Wang, S. Q.; Chen, Y. C. Adsorption and desorption of Cu(II), Zn(II), Pb(II), and Cd(II) on the soils amended with nanoscale hydroxyapatite. *Environ. Prog. Sustain. Energy* **2010**, *29* (2), 233−241.

(10) Zhang, Z.; Li, M.; Chen, W.; Zhu, S.; Liu, N.; Zhu, L. Immobilization of lead and cadmium from aqueous solution and contaminated sediment using nano-hydroxyapatite. *Environ. Pollut.* **2010**, *158* (2), 514−519.

(11) Islam, M.; Mishra, P. C.; Patel, R. Arsenate removal from aqueous solution by cellulose-carbonated hydroxyapatite nanocomposites. *J. Hazard. Mater.* **2011**, *189* (3), 755−763.

(12) Handley-Sidhu, S.; Renshaw, J. C.; Moriyama, S.; Stolpe, B.; Mennan, C.; Bagheriasl, S.; Yong, P.; Stamboulis, A.; Paterson-Beedle, M.; Sasaki, K.; Pattrick, R. A. D.; Lead, J. R.; Macaskie, L. E. Uptake of Sr^{2+} and Co^{2+} into biogenic hydroxyapatite: Implications for biomineral ion exchange synthesis. *Environ. Sci. Technol.* **2012**, *45* (16), 6985−6990.

(13) Ewing, R. C.; Wang, L. M. Phosphates as nuclear waste forms. *Rev. Mineral. Geochem.* **2002**, *48* (1), 673−699.

(14) White, A. F.; Brantley, S. L. Chemical weathering of silicate minerals. *Rev. Mineral.* **1995**, *31*, 1−583.

(15) Torrent, J.; Barron, V.; Schwertmann, U. Phosphate adsorption and desorption by goethites differing in crystal morphology. *Soil Sci. Soc. Am. J.* **1990**, *54* (4), 1007−1012.

(16) Frossard, E.; Brossard, M.; Hedley, M. J.; Meterell, A. Reactions controlling the cycling of P in soils. In Tiessen, H., Ed.; *Phosphorus in the Global Environment*; Wiley: New York, SCOPE 54, 1995; Ch. 7, pp 107−137

(17) Schwertmann, U.; Cornell, R. M. *Iron Oxides in the Laboratory: Preparation and Characterization*, 2nd ed.; Wiley-VCH Verlag GmbH: Berlin, 2000.

(18) van der Zee, C.; Roberts, D. R.; Rancourt, D. G.; Slomp, C. P. Nanogoethite is the dominant reactive oxyhydroxide phase in lake and marine sediments. *Geology* **2003**, *31* (11), 993−996.

(19) Rick, A. R.; Arai, Y. Role of natural nanoparticles in phosphorus transport processes in ultisols. *Soil Sci. Soc. Am. J.* **2011**, *75* (2), 335−347.

(20) Ryan, J. N.; Elimelech, M. Colloid mobilization and transport in groundwater. *Colloids Surf., A* **1996**, *107*, 1−56.

(21) Walshe, G. E.; Pang, L.; Flury, M.; Close, M. E.; Flintoft, M. Effects of pH, ionic strength, dissolved organic matter, and flow rate on the co-transport of MS2 bacteriophages with kaolinite in gravel aquifer media. *Water Res.* **2010**, *44* (4), 1255−1269.

(22) Chowdhury, I.; Cwiertny, D. W.; Walker, S. L. Combined factors influencing the aggregation and deposition of nano-TiO_2 in the presence of humic acid and bacteria. *Environ. Sci. Technol.* **2012**, *46* (13), 6968−6976.

DOI: 10.1021/acs.est.5b01210
Environ. Sci. Technol. 2015, 49, 8461−8470

(23) Zhou, D. X.; Abdel-Fattah, A. I.; Keller, A. A. Clay particles destabilize engineered nanoparticles in aqueous environments. *Environ. Sci. Technol.* **2012**, *46* (14), 7520−7526.
(24) Cai, L.; Tong, M. P.; Ma, H.; Kim, H. Cotransport of titanium dioxide and fullerene nanoparticles in saturated porous media. *Environ. Sci. Technol.* **2013**, *47* (11), 5703−5710.
(25) Kosmulski, M. The pH-dependent surface charging and points of zero charge: V. Update. *J. Colloid Interface Sci.* **2011**, *353* (1), 1−15.
(26) Motskin, M.; Wright, D. M.; Muller, K.; Kyle, N.; Gard, T. G.; Porter, A. E.; Skepper, J. N. Hydroxyapatite nano and microparticles: Correlation of particle properties with cytotoxicity and biostability. *Biomaterials* **2009**, *30* (19), 3307−3317.
(27) Bose, P.; Sharma, A. Role of iron in controlling speciation and mobilization of arsenic in subsurface environment. *Water Res.* **2002**, *36* (19), 4916−4926.
(28) Therezien, M.; Thill, A.; Wiesner, M. R. Importance of heterogeneous aggregation for NP fate in natural and engineered systems. *Sci. Total Environ.* **2014**, *485*−*486*, 309−318.
(29) Huynh, K. A.; McCaffery, J. F.; Chen, K. L. Heteroaggregation of multiwalled carbon nanotubes and hematite nanoparticles: Rates and mechanisms. *Environ. Sci. Technol.* **2012**, *46* (11), 5912−5920.
(30) Elimelech, M.; Gregory, J.; Jia, X.; Williams, R. *Particle Deposition and Aggregation: Measurement, Modelling and Simulation*; Butterworth-Heinemann: Woburn, MA, 1995.
(31) Petosa, A. R.; Jaisi, D. P.; Quevedo, I. R.; Elimelech, M.; Tufenkji, N. Aggregation and deposition of engineered nanomaterials in aquatic environments: Role of physicochemical interactions. *Environ. Sci. Technol.* **2010**, *44* (17), 6532−6549.
(32) Zhang, P.; Ryan, J. A. Formation of pyromorphite in anglesite-hydroxyapatite suspensions under varying pH conditions. *Environ. Sci. Technol.* **1998**, *32* (21), 3318−3324.
(33) Stumm, W.; Morgan, J. J. *Aquatic Chemistry: Chemical Equilibria and Rates in Natural Waters*, 3rd ed.; John Wiley & Sons, Ltd: New York, 1995.
(34) Nebbioso, A.; Piccolo, A. Molecular characterization of dissolved organic matter (DOM): A critical review. *Anal. Bioanal. Chem.* **2013**, *405* (1), 109−124.
(35) Philippe, A.; Schaumann, G. E. Interactions of dissolved organic matter with natural and engineered inorganic colloids: A review. *Environ. Sci. Technol.* **2014**, *48* (16), 8946−8962.
(36) Wang, D. J.; Bradford, S. A.; Harvey, R. W.; Gao, B.; Cang, L.; Zhou, D. M. Humic acid facilitates the transport of ARS-labeled hydroxyapatite nanoparticles in iron oxyhydroxide-coated sand. *Environ. Sci. Technol.* **2012**, *46* (5), 2738−2745.
(37) Tiller, C. L.; O'Melia, C. R. Natural organic matter and colloidal stability: Models and measurements. *Colloids Surf., A* **1993**, *73*, 89−102.
(38) Piccolo, A. The supramolecular structure of humic substances. *Soil Sci.* **2001**, *166* (11), 810−832.
(39) Louie, S. M.; Spielman-Sun, E. R.; Small, M. J.; Tilton, R. D.; Lowry, G. V. Correlation of the physicochemical properties of natural organic matter samples from different sources to their effects on gold nanoparticle aggregation in monovalent electrolyte. *Environ. Sci. Technol.* **2015**, *49* (7), 2188−2198.
(40) Chin, Y. P.; Aiken, G.; O'Loughlin, E. Molecular weight, polydispersity, and spectroscopic properties of aquatic humic substances. *Environ. Sci. Technol.* **1994**, *28* (11), 1853−1858.
(41) Schlautman, M. A.; Morgan, J. J. Adsorption of aquatic humic substances on colloidal-size aluminum oxide particles: Influence of solution chemistry. *Geochim. Cosmochim. Acta* **1994**, *58* (20), 4293−4303.
(42) Chen, K. L.; Elimelech, M. Influence of humic acid on the aggregation kinetics of fullerene (C_{60}) nanoparticles in monovalent and divalent electrolyte solutions. *J. Colloid Interface Sci.* **2007**, *309*, 126−134.
(43) Bradford, S. A.; Yates, S. R.; Bettahar, M.; Simunek, J. Physical factors affecting the transport and fate of colloids in saturated porous media. *Water Resour. Res.* **2002**, *38* (12), 63-1−63-12, DOI: 10.1029/2002WR001340.
(44) Kretzschmar, R.; Sticher, H. Transport of humic-coated iron oxide colloids in a sandy soil: Influence of Ca^{2+} and trace metals. *Environ. Sci. Technol.* **1997**, *31* (12), 3497−3504.
(45) Kuhnen, F.; Barmettler, K.; Bhattacharjee, S.; Elimelech, M.; Kretzschmar, R. Transport of iron oxide colloids in packed quartz sand media: Monolayer and multilayer deposition. *J. Colloid Interface Sci.* **2000**, *231* (1), 32−41.
(46) Huynh, K. A.; McCaffery, J. F.; Chen, K. L. Heteroaggregation reduces antimicrobial activity of silver nanoparticles: Evidence for nanoparticle−cell proximity effects. *Environ. Sci. Technol. Lett.* **2014**, *1* (9), 361−366.
(47) Harter, T.; Wagner, S.; Atwill, E. R. Colloid transport and filtration of Cryptosporidium parvum in sandy soils and aquifer sediments. *Environ. Sci. Technol.* **2000**, *34* (1), 62−70.
(48) Su, C.; Puls, R. W.; Krug, T. A.; Watling, M. T.; O'Hara, S. K.; Quinn, J. W.; Ruiz, N. E. A two and half-year-performance evaluation of a field test on treatment of source zone tetrachloroethene and its chlorinated daughter products using emulsified zero valent iron nanoparticles. *Water Res.* **2012**, *46* (16), 5071−5084.
(49) Phull, S. S.; Newman, A. P.; Lorimer, J. P.; Pollet, B.; Mason, T. J. The development and evaluation of ultrasound in the biocidal treatment of water. *Ultrason. Sonochem.* **1997**, *4* (2), 157−164.
(50) Murphy, J.; Riley, J. P. A modified single solution method for the determination of phosphate in natural waters. *Anal. Chem. Acta* **1962**, *27*, 31−36.
(51) Schwertmann, U.; Cambier, P.; Murad, E. Properties of goethites of varying crystallinity. *Clays Clay Miner.* **1985**, *33* (5), 369−378.
(52) Handler, R. M.; Frierdich, A. J.; Johnson, C. M.; Rosso, K. M.; Beard, B. L.; Wang, C.; Latta, D. E.; Neumann, A.; Pasakarnis, T.; Premaratne, W. A. P. J.; Scherer, M. M. Fe(II)-catalyzed recrystallization of goethite revisited. *Environ. Sci. Technol.* **2014**, *48* (19), 11302−11311.
(53) Gibson, I. R.; Best, S. M.; Bonfield, W. Chemical characterization of silicon-substituted hydroxyapatite. *J. Biomed. Mater. Res.* **1999**, *44* (4), 422−428.
(54) Wang, D. J.; Bradford, S. A.; Paradelo, M.; Peijnenburg, W. J. G. M.; Zhou, D. M. Facilitated transport of copper with hydroxyapatite nanoparticles in saturated sand. *Soil Sci. Soc. Am. J.* **2012**, *76* (2), 375−388.
(55) Tipping, E. The adsorption of aquatic humic substances by iron oxides. *Geochim. Cosmochim. Acta* **1981**, *45* (2), 191−199.
(56) Weng, L. P.; Van Riemsdijk, W. H.; Hiemstra, T. Humic nanoparticles at the oxide−water interface: Interactions with phosphate ion adsorption. *Environ. Sci. Technol.* **2008**, *42* (23), 8747−8752.
(57) Xie, B.; Xu, Z.; Guo, W.; Li, Q. Impact of natural organic matter on the physicochemical properties of aqueous C_{60} nanoparticles. *Environ. Sci. Technol.* **2008**, *42* (8), 2853−2859.
(58) Zhang, W.; Rattanaudompol, U. S.; Li, H.; Bouchard, D. Effects of humic and fulvic acids on aggregation of aqu/nC_{60} nanoparticles. *Water Res.* **2013**, *47* (5), 1793−1802.
(59) Liu, D.; Johnson, P. R.; Elimelech, M. Colloid deposition dynamics in flow-through porous media: Role of electrolyte concentration. *Environ. Sci. Technol.* **1995**, *29* (12), 2963−2973.
(60) Chen, G.; Liu, X.; Su, C. Distinct effects of humic acid on transport and retention of TiO_2 rutile nanoparticles in saturated sand columns. *Environ. Sci. Technol.* **2012**, *46* (13), 7142−7150.
(61) Yao, K. M.; Habibian, M. M.; O'Melia, C. R. Water and waste water filtration: Concepts and applications. *Environ. Sci. Technol.* **1971**, *5* (11), 1105−1112.
(62) Tufenkji, N.; Elimelech, M. Correlation equation for predicting single-collector efficiency in physicochemical filtration in saturated porous media. *Environ. Sci. Technol.* **2004**, *38* (2), 529−536.
(63) Jiang, X.; Tong, M.; Lu, R.; Kim, H. Transport and deposition of ZnO nanoparticles in saturated porous media. *Colloids Surf., A* **2012**, *401*, 29−37.
(64) Wang, D.; Su, C.; Liu, C.; Zhou, D. Transport of fluorescently labeled hydroxyapatite nanoparticles in saturated granular media at

DOI: 10.1021/acs.est.5b01210
Environ. Sci. Technol. 2015, 49, 8461−8470

environmentally relevant concentrations of surfactants. *Colloids Surf., A* **2014**, *457*, 58−66.
(65) Tufenkji, N.; Elimelech, M. Breakdown of colloid filtration theory: Role of the secondary energy minimum and surface charge heterogeneities. *Langmuir* **2005**, *21* (3), 841−852.
(66) Wang, Y.; Kim, J. H.; Baek, J. B.; Miller, G. W.; Pennell, K. D. Transport behavior of functionalized multi-wall carbon nanotubes in water-saturated quartz sand as a function of tube length. *Water Res.* **2012**, *46* (14), 4521−4531.
(67) Liang, Y.; Bradford, S. A.; Simunek, J.; Heggen, M.; Vereecken, H.; Klumpp, E. Retention and remobilization of stabilized silver nanoparticles in an undisturbed loamy sand soil. *Environ. Sci. Technol.* **2013**, *47* (21), 12229−12237.
(68) Wang, D. J.; Ge, L. Q.; He, J. Z.; Zhang, W.; Jaisi, D. P.; Zhou, D. M. Hyperexponential and nonmonotonic retention of polyvinylpyrrolidone-coated silver nanoparticles in an ultisol. *J. Contam. Hydrol.* **2014**, *164*, 35−48.
(69) Wang, Y. G.; Kim, J. H.; Baek, J. B.; Miller, G. W.; Pennell, K. D. Transport behavior of functionalized multi-wall carbon nanotubes in water-saturated quartz sand as a function of tube length. *Water Res.* **2012**, *46* (14), 4521−4531.
(70) Jones, D. L. Organic acids in the rhizosphere - A critical review. *Plant Soil* **1998**, *205* (1), 25−44.

DOI: 10.1021/acs.est.5b01210
Environ. Sci. Technol. 2015, 49, 8461−8470